SMAR 2019 – Fifth Conference on Smart Monitoring,
Assessment and Rehabilitation of Civil Structures

SMAR 2019

Feasibility of Superelastic Large Diameter Copper-Aluminum-Manganese SMA Bars in Bridge Columns

Saiid SAIIDI [1] and Evan JORDAN[2]
[1] University of Nevada, Reno, Civil Engineering (258), UNR, Reno, NV 89557, USA
[2] Staff engineer, Magnusson Klemencic Associates up in Seattle, Washington, USA

Contact e-mail: saiidi@unr.edu

ABSTRACT: Superelastic Copper-Aluminum-Manganese (CAM) reinforcing bars present an attractive alternative to steel bars in reinforced concrete structures not only because they provide resistance and ductility under earthquake loads, but they also minimize residual displacements. The length of available large-diameter CAM bars is limited and hence the bars should be spliced. The most efficient splicing method is to use headed bar couplers because no machining of the CAM bars is necessary using these couplers. This artilce presents the measured response of spliced 30-mm diameter CAM bars using headed bar couplers subjected to monotonic and cyclic loads. It is shown that, while the results are promissing, further development is necessary to obtain consistent performance.

1 INTRODUCTION

Superelastic shape memory alloy (SMA) bars have been proven to be a viable alternative to provide recentering for bridge columns subjected to strong earthquake loading. Recentering of bridges following strong earthquakes improves bridge resiliency and the probability of keeping the bridge in service. Of different types of SMA bars, development of Nickel-Titanium (NiTi) alloy bars is more mature than other types. Reinforced concrete bridge columns reinforced with NiTi bars of 30 mm diameter in the plastic hinge have been studied Tazarv and Saiidi (2015) and implemented in a three-span bridge in Seattle, Washington, Baker et al (2018), the first such application in the world as of this writing. Alternative superelastic SMA bars incorporating Copper, Aluminum, and Manganese (CAM), have been emerging that are substantially less expensive than NiTi. The mechanical properties of CAM are different from those of NiTi and steel. Table 1 summarizes the basic properties of each. It can be seen that the modulus of elasticity and the yield strength of CAM are substantially lower than those of NiTi and steel.

Table 1: Expected Strength Properties of CAM, Nitinol, and Gr. 60 Steel

Property	CAM	NiTi	A706, Grade 60
Austenite Modulus* (GPa)	28.0	38.0	200.0
Austenite Yield Stress* (MPa)	166.0	380.0	470.0
Ultimate Stress (MPa)	310.0	896.0	690.0

*Austenite refers to the properties associated with the initial loading

Testing and analysis of columns incorporating 15-mm diameter CAM bars have demonstrated their feasibility and effectiveness in recentering of bridge columns subjected to strong earthquakes that permanently displace the top of the columns. For field application, large-diameter CAM bars are needed. Superelastic CAM bars have been developed with a diameter of 30 mm. The bars are forged to a larger diameter under high temperatures and then are cold drawn to 30-mm dimeter under a lower temperature. For a variety of reasons, the maximum length for the bars that have been developed is 300 mm. The necessary length for a typical bridge column is 1 m or more. The purpose of the study presented in this article was to determine the feasibility of splicing 30-mm CAM bars to form a longer CAM bar for application in column plastic hinges.

2 SPLICE TYPES

Different types of splices are available to link deformed steel bars and can be used to link SMA bars. Figure 1 shows the most common splices. Of these, types a- shear screw, c- headed bar, and d- threaded bar have been used to splice SMA bars with steel bars. Type (a) has seen only limited testing. Type (d) requires machining of the ends and reducing the diameter between the couplers to avoid failure at the threads. This type has the disadvantage of wasting some of the material in the part with reduced diameter. Therefore, type (c) was selected because it has been used in past studies for splicing both large-diameter NiTi bars and small- diameter CAM bars, all to link the bars with steel bars. Type (c) has not been used to splice large-diameter CAM bars to either steel or other large-diameter CAM bars. Splicing large-diameter CAM bars presented in this article is the first of such application as of this writing.

3 TEST SPECIMENS

Two test specimens each consisting of two No. 10 steel bars and two, 30-mm diameter CAM bars were prepared. The CAM specimens were inserted into the couplers and were twisted to the manufacturer specified torque of 135.6 N-m. This torque is intended to pre-compress the CAM bar heads such that the misalignments of the heads within the coupler is minimized. The length of each CAM bar prior to flattening the ends was 300 mm. The headed bar splice [Type (c) in Figure 1] was used. Figure 2 and 3 show the layout and a photo of one of the specimens, respectively. Note that the flattening process reduced the total length of each bar to 247.5 mm. Four strain gages were installed at mid-length of each CAM bar around the section to measure tensile strains and track any bending stresses when the specimens are subjected to tensile loading. The overall strain of the combined CAM bars and the splices was measured using a pair of linear variable differential transformer (Figure 4) with a gage length of 668 mm.

4 TEST PROCEDURE

Specimen 1 was subjected to tensile monotonic loading to failure. The second specimen was subjected to tensile half-cyclic loading to failure. The loading rate was at a strain of of 0.2%/sec. The monotonic loading consisted of pulling the specimen. The multi half-cycle testing consisted of loading the specimen twice to gradually increasing peak strains, releasing the load to near zero, reloading to the next higher strain up to a target strain of 8% and then pull to failure. The unloading did not proceed to zero load because of concern about change of alignment of the CAM and steel bars. The target strain amplitudes were 0.25%, 0.5%, 0.75%, 1%, 2%, 3%, 4%, 5%, 6%, 7%, 8%. The loading proceeded until the maximum strain that the specimen could resist.

Figure 1. Available splice types.

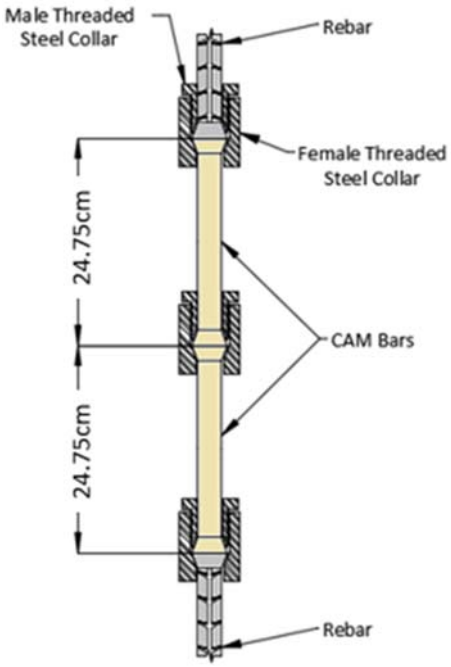

Figure 2. Test specimen components.

Figure 3. Instrumented test specimens.

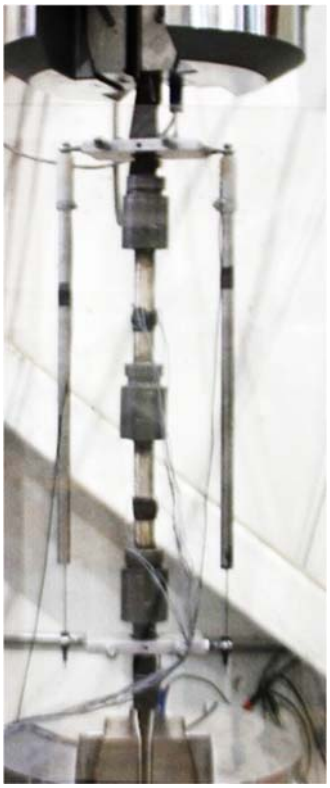

Figure 4. Test setup.

5 TEST RESULTS

5.1 Results under monotonic loading

Figure 5 shows the fractured specimen 1 that was tested under monotonic tensile loading. Figure a shows that the failure occurred near the middle coupler connecting the two CAM bars. The cause of failure appeared to be due to stress concentration at the flattened end of the fractured bar. The failure could be because of uneven flattening of the bar end or change in CAM fracture strain due to the heating of the bar end. The latter is the less likely reason considering the fracture location of specimen 2 discussed in subsequent sections. It is believed that uneven surface of the flattened part of the bar end was the primary factor that led to eccentric loading during the test. Note that the other CAM bar and the remaining two couplers were not damaged.

Figure 6 presents the average stress-strain curves based on the strains gages on the top and bottom bars in comparison with the data from the LVDTs. Comparing the strain gage data for the top and bottom (where fracture occurred) bars, major differences are observed once the elastic limit is exceeded. The top bar exhibits a lower "yield" stress, but the post-yield stiffness was nearly the same for the two bars. The top bar exhibited substantial strain hardening at approximately 8%, an effect typically expected in CAM bars. The same was not observed in the bottom bars. Only limited strain hardening occurred at 10% strain. The LVDT data essentially represent the average behavior of the top and bottom bars.

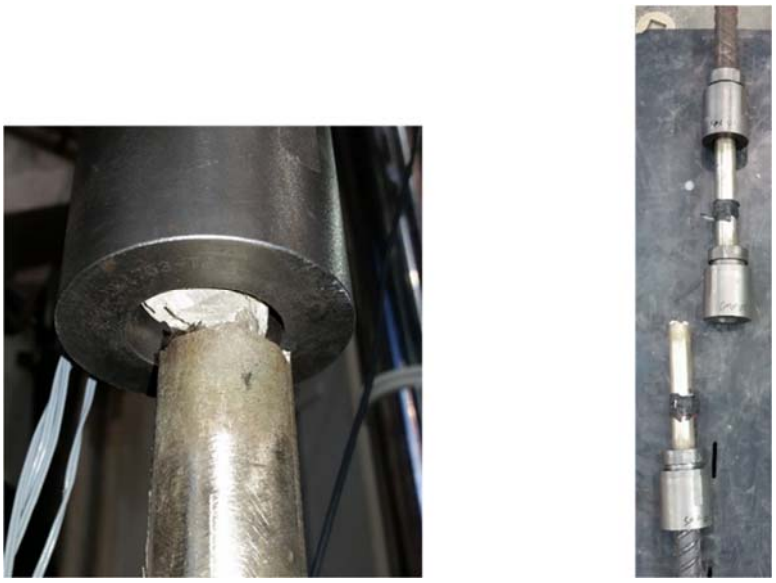

(a) (b)

Figure 5. Specimen 1 after testing under monotonic loading.

The variation between the behavior of the two bars is attributed to the differences in the flattened ends and the possible effect of heating during the heading process, which most likely varied between the two bars. The heat affected strain hardening. The relatively large fracture strain of 17% shows that the heating did not adversely affect the bar ductility by a substantial amount.

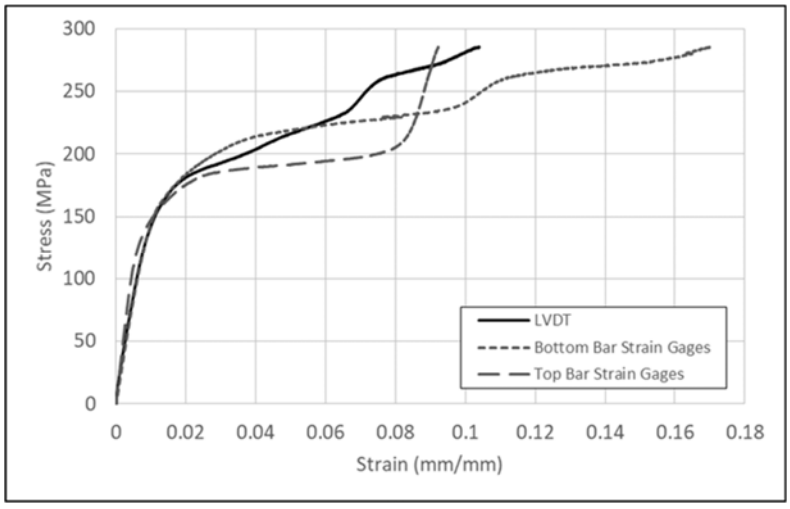

Figure 6. Measured stress-strain relationship under monotonic loads.

5.2 Results under cyclic loading

The second specimen was tested under half-cyclic loading with the target strains that were listed in Section 4. The actual strains were lower by approximately 20% at each cycle due to mostly deformations of and settling of the headed ends within the couplers. Testing was continued until the specimen failed at a strain of 4.2% as measured by the LVDTs.

Figure 7 the fracture of the specimen, and Figure 8 shows the close up of the fracture plane. Failure occurred towards the middle of the bottom CAM bar, meaning that, unlike the first specimen , failure did not occur due to stress concentration in the flattened ends. As can be seen in Figure 8, the fracture surfaces are highly variable and jagged, indicating somewhat of a brittle failure mode. This was confirmed by the relatively small measured fracture strain.

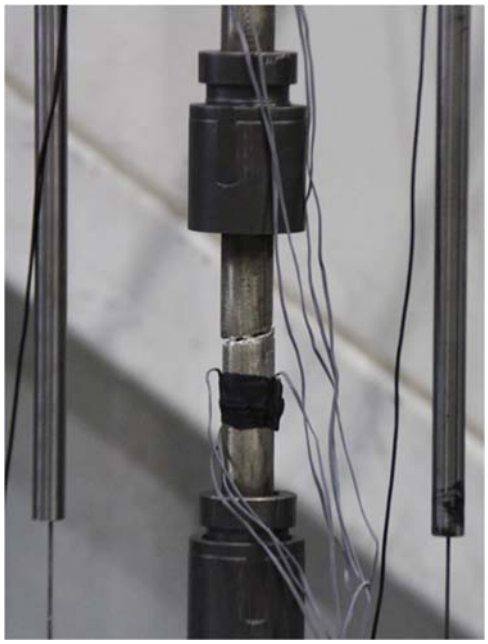

Figure 7. Fracture of specimen under cyclic loading.

(a) (b)

Figure 8. Close up of the fracture surfaces.

Figure 9 shows the stress-strain cyclic response based on the average data obtained using the LVDT pair. It can be seen that the specimen had excellent superelastic behavior, having minimal residual strains after each cycle. The curves depicting the strain recovery are comparable to curves from testing of smaller CAM bars under similar cyclic loading protocol in Varela and

Saiidi (2014), Hosseini et al. (2015), and Kise et al. (2018). The area within the curves also appears to be comparable to those seen in previous research on smaller diameter CAM bars.

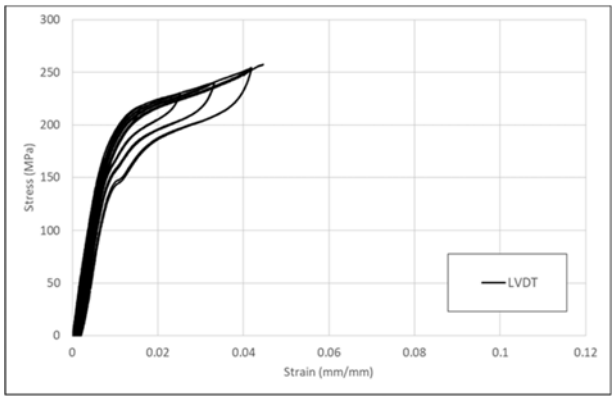

Figure 9. Measured overall stress-strain relationship under half cyclic load.

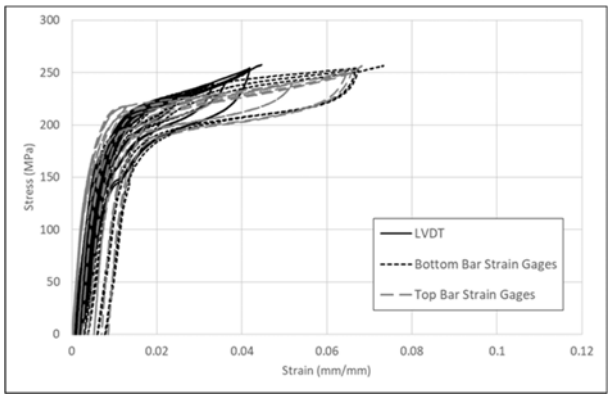

Figure 10. Measured stress-strain relationships using LVDT and strain gages.

Figure 10 presents the LVDT stress-strain data superimposed on the average data for the top and bottom bars obtained from strain gages. The strain gage data reflect the stain in the CAM bar without the influence of deformation at the couplers. The graphs show that the stress-strain relationships for the top and bottom bars are comparable. Also it can be seen that the fracture strain obtained from strain gages is 7.3%, which is substantially higher the overall strain measured by the LVDTs. The residual strains obtained from strain gages are greater than those obtained from LVDTs because part of the apparent strain in the LVDT data is due to opening at the coupler gap. This gap is fully recovered upon unloading. Also note that neither bar experienced martensite detwinning upon approaching strains exceeding 7%, as was experienced in one of the bars subjected to monotonic loading, indicating variability in micro-structure among the samples.

Figure 11 shows the envelope of the measured stress-strain curves under cyclic loads superimposed on the data from specimen 1. While specimen 2 has a higher initial stiffness, it fails at around 4.5% strain, indicating a substantial reduction of the ultimate strain capacity due to the cyclic loads. The higher initial stiffness of the cyclic test result is due to training that takes place under cyclic loads with smaller strains of up to 2%. Smaller diameter bars of 13 mm have

been successfully tested to near 40% ultimate strains while enduring the same cyclic protocol as that listed in section 4, Kise et al (2018). This loss of ductility from cyclic loading is perhaps due to uneven heading process, the large diameter, and the effect of heating the ends on the bars that were relatively short considering their large diameter.

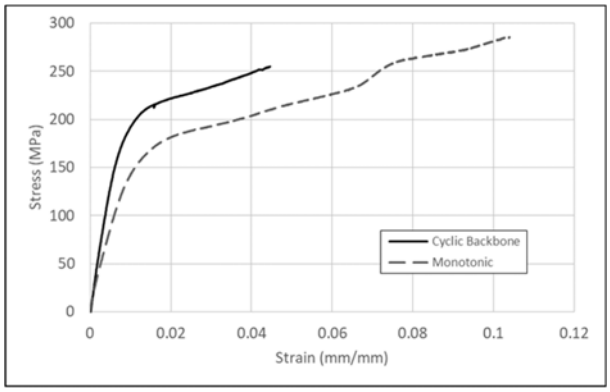

Figure 11. Envelopes of stress-strain curves obtained from LVDTs.

6 CONCLUSIONS

The exploratory study of spliced large-diameter CAM bars revealed that further research and development of these bars are needed before spliced bars are utilized in bridge column models to be tested under seismic loads. The ultimate strain capacity of the large-diameter CAM bars was substantially lower than that observed in smaller diameter CAM bars, although strain recovery, the apparent yield stress, and the ultimate strengths were comparable. There appears to be significant reduction in the ultimate strain due to difficulty in uniformly flattening the ends under high heat and perhaps the negative influence of the heat over the rest of the bar.

7 REFERENCES

Tazarv, M. and M. Saiidi, 2015, Low-Damage Precast Columns for Accelerated Bridge Construction in High Seismic Zones, *Journal of Bridge Engineering, ASCE,* 20(3): 04015056-1-13.

Baker, T., M. Saiidi, B. Nakashoji, J. Bingle, T. Moore, and B. Khaleghi, 2018, Precast Spliced Girder Bridge in Washington State using Superelastic Materials in Bridge Columns to Improve Seismic Resiliency - From Research to Practice, *PCI Journal, Precast/Prestressed Concrete Institute*, 57-71.

Hosseini, F., B. Gencturk, S. Lahpour, and D. Ibague, 2015, An Experimental Investigation of Innovative Bridge Columns with Engineered Cementitious Composites and Cu–Al–Mn Super-elastic Alloys, *Smart Materials and Structures*, 24(8).

Kise, S., A. Mohebbi, M. Saiidi, T. Omori, R. Kainuma, K. Shrestha, and Y. Araki, 2018, Mechanical Splicing of Superelastic Cu-Al-Mn Bars with Headed Ends, *Journal of Smart Materials and Structures*, 27(6).

Varela, S., and M. Saiidi, 2014, Dynamic Performance of Innovative Bridge Columns with Superelastic CuAlMn Shape Memory Alloy and ECC, *International Journal of Bridge Engineering* 2(3).